

# Non-destructive testing of building walls using active infrared thermography

by L.Ibos, M. Larbi Youcef, A. Mazioud, S. Datcu and Y. Candau

*\*CERTES, Université Paris XII Val de Marne, Créteil, France*

## Abstract

This work concerns the development of a new method for the non-destructive testing of building walls. The final objective is to apply this method to test of building thermal insulation. The proposed method uses active infrared thermography. We are more especially interested in the determination of the thermal resistance of multi-layered walls. In this paper, we present the first results obtained concerning the determination of the experimental protocol and its application to the characterisation of samples in laboratory conditions.

## 1 Introduction

Active infrared thermography consists in monitoring surface temperatures of a body submitted to some kind of radiant heat excitation; as such it can provide an ideal non-invasive exploring technique. A possible field of application of this technique is in testing the composition of walls in existing buildings [1]. We are more especially interested in the determination of the thermal resistance of multi-layered walls [2]. This paper presents a simple experimental protocol and its application to the characterisation of two-layer samples.

## 2 Experimental setup

### 2.1 Samples

The structure of the two samples investigated is presented in figure 1. These samples are composed of two layers: one layer made of plaster and one made of expanded polystyrene. For the first sample, the thickness of the plaster layer is equal to 1 cm, whereas the thickness of the polystyrene layer is equal to 2 cm. In the second sample, the thickness of the plaster layer is continuously varying along the horizontal direction from 0.5 cm (in the left part of the sample) to 2.5 cm (in the right part of the sample). The total thickness of the sample is equal to 5.5 cm. The bottom part of the plaster layer (front face of the sample) is coated using a black paint of known emissivity (0.97), in order to obtain an accurate estimation of the surface temperature and to minimize the influence of the reflected infrared flux.

The thermophysical properties of plaster and expanded polystyrene are given in table 1. These values are literature values [1,2,3]; no specific experiments were performed to obtain the exact values of these properties with their uncertainties. Moreover, a large range of values can be found in the literature, especially concerning the thermal conductivity and diffusivity of plaster.

**Table 1.** Thermophysical properties of plaster and expanded polystyrene [1,2,3]

Material	Plaster	Expanded Polystyrene
$k$ ( $W.m^{-1}.K^{-1}$ )	0.30	0.033
$a$ ( $m^2.s^{-1}$ )	$4.17 \cdot 10^{-7}$	$5.89 \cdot 10^{-7}$
$Cp$ ( $J.kg^{-1}.K^{-1}$ )	900	1400
$\rho$ ( $kg.m^{-3}$ )	800	40

**2.2 Experimental protocol**

The experimental set-up is described in figure 2 [4]. The front side of the sample is heated using two halogen lamps of constant power  $P$  during a finite exposure time  $t_e$ . The sample front face temperature is measured using an infrared camera (model AGEMA 570) during the excitation pulse (heating) and also during the subsequent cooling until time  $t_f = 4t_e$ . For the first sample,  $t_e$  was fixed equal to 300s, whereas a value of  $t_e = 1800s$  was used for the second sample. The distance between the camera and the sample surface was fixed to 1m. The use of a short distance allows assuming that the atmospheric transmission factor is close to 1 in the camera spectral range (7.5 – 13  $\mu m$ ).

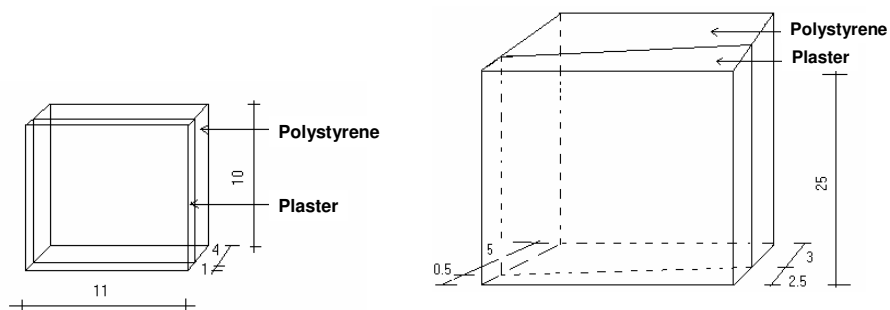


**Fig. 1.** Schematic view of the samples investigated: first sample (left), second sample (right); dimensions given in cm.

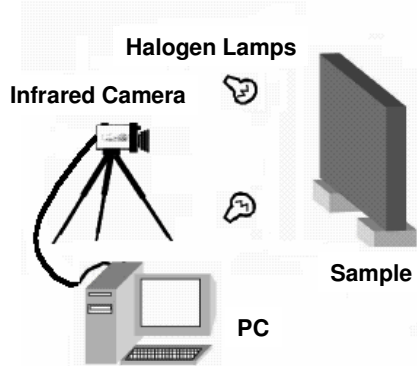


**Fig. 2.** Description of the experimental set-up

Infrared images taken at the end of the thermal excitation ( $t = 300\text{s}$  for the first sample and  $t = 1800\text{s}$  for the second one) are presented in figures 3 and 4. The square zones labelled AR0i represent the regions of the surface that were used for the analysis presented further in this paper. A mean temperature value was computed for each zone and for each image in order to obtain the evolution of the surface temperature with time.



*Fig. 3. Infrared image of the first sample at the end of the thermal excitation.*

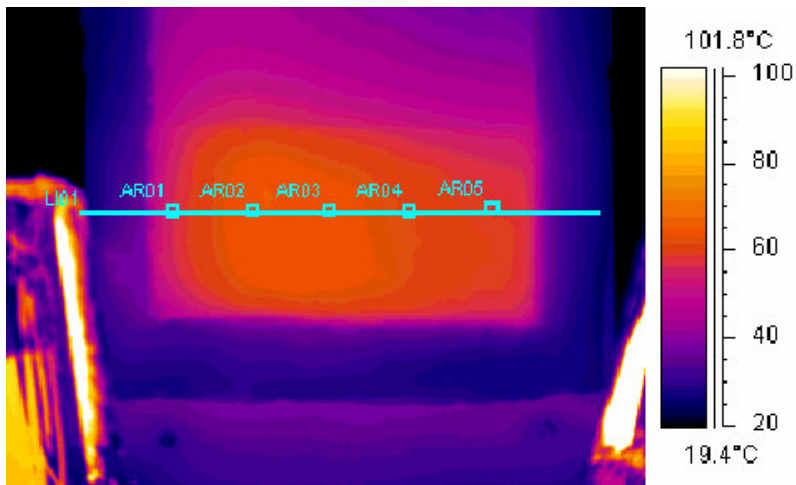


*Fig. 4. Infrared image of the second sample at the end of the thermal excitation.*

### 3 Thermal models

Two thermal models were used to analyse the evolution of the sample surface temperature, and to obtain an estimation of the thermophysical properties of the first layer (plaster). In both cases, we considered a 1D heat transfer in the sample. In the first model, we considered that the interface between the plaster layer and the polystyrene layer is adiabatic, due to the high thermal resistance of the polystyrene. In the second model, we considered the case of a semi-infinite body. In both cases, heat exchanges on the front surface of the sample are taken into account using a global heat exchange coefficient  $h$ . This coefficient is assumed to be constant during an experiment.

#### 3.1 Adiabatic surface model

The heat transfer equation and the boundary and limit conditions are given by the following relationships:

$$\frac{\partial^2 \theta}{\partial x^2} = \frac{1}{a} \frac{\partial \theta}{\partial t}, \quad t = 0, \quad \theta(x, 0) = 0 \quad (1)$$

$$x = 0, \quad -k \frac{\partial \theta(0, t)}{\partial x} + h \theta(0, t) = f_1(t), \quad f_1(t) = \begin{cases} P, & t \leq t_e \\ 0, & t > t_e \end{cases} \quad (2)$$

$$x = L, \quad k \cdot \frac{\partial \theta(L, t)}{\partial x} = 0 \quad (3)$$

where  $\theta(x, t)$  is the temperature rise at position  $x$  and time  $t$ ,  $k$  and  $a$  are respectively the thermal conductivity and diffusivity of the first layer,  $L$  is the first layer thickness,  $P$  is the excitation power absorbed by the sample surface and  $h$  is the heat exchange coefficient on the front side of the sample.

The solution on the sample surface ( $x = 0$ ) is given by:

$$\theta(0, t) = C \cdot \sum_{n=0}^{\infty} \frac{(1 - e^{-F_0 \lambda_n t})}{\lambda_n^2 + NB + NB^2} \Bigg|_{t \leq 1}, \quad (4)$$

$$\theta(0, t) = C \cdot \sum_{n=0}^{\infty} \frac{(e^{F_0 \lambda_n} - 1) e^{-F_0 \lambda_n t}}{\lambda_n^2 + NB + NB^2} \Bigg|_{t > 1}$$

with

$$tg(\lambda_n) = \frac{NB}{\lambda_n}, \quad \lambda_n = b_n L, \quad t' = \frac{t}{t_e} \quad (5)$$

$NB$  is the Biot number:

$$NB = \frac{hL}{k} \quad (6)$$

$Fo_e$  is the Fourier number computed at  $t = t_e$ :

$$Fo_e = \frac{at_e}{L^2} \quad (7)$$

And  $C$  is the maximum amplitude of the temperature rise:

$$C = \frac{2PL}{k} \quad (8)$$

### 3.2 Semi-infinite body model

In that case, the solution is given by [5]:

$$\theta(x,t) = \alpha \cdot \left( \operatorname{erfc}\left(\frac{\gamma}{2 \cdot \sqrt{t}}\right) - e^{(\beta \cdot \gamma + \beta^2 \cdot t)} \cdot \operatorname{erfc}\left(\frac{\gamma}{2 \cdot \sqrt{t}} + \beta \cdot \sqrt{t}\right) \right) \quad (9)$$

with:

$$\alpha = \frac{P}{h}; \quad \beta = \frac{h}{e}; \quad \gamma = \frac{x}{\sqrt{a}} \quad (10)$$

where  $e$  is the effusivity of the material.

The solution on the sample surface ( $x = 0$ ) is given by:

$$\theta(0,t) = \alpha \cdot \left( 1 - e^{\beta^2 \cdot t} \cdot \operatorname{erfc}(\beta \cdot \sqrt{t}) \right) \quad (11)$$

### 3.3 Parameters identification

In both cases (adiabatic surface model and semi-infinite body model), the parameters are estimated using a least-square minimization of the difference between the temperature measured on the sample surface sample and the temperature given by the models.

In the case of the adiabatic surface model, the estimated parameters are the Biot number  $NB$ , the Fourier number  $Fo_e$  and the amplitude  $C$ . The estimation is performed using all experimental data (between  $t = 0$  and  $t = t_i$ ), *i.e.* during the

excitation and the subsequent cooling. Then, thermophysical properties can be computed knowing the value of the heat exchange coefficient  $h$ , the excitation time  $t_e$  and the first layer thickness  $L$ .

In the case of the semi-infinite body model, two parameters are estimated:  $\alpha$  and  $\beta$ . The estimation is performed only during the excitation period and for measurement times increasing progressively from  $t = 0$  to  $t = t_e$ . The aim is here to define a characteristic time  $t_c$ , corresponding to the time when the thermal model becomes invalid. We will see later in this paper that this characteristic time can be correlated to the position of the interface between the plaster layer and the polystyrene layer.

## 4 Results

### 4.1 Adiabatic surface model

The identification results using the adiabatic surface model are presented in tables 2 and 3 for the first and second sample respectively. We have reported the results obtained for the five measurement points analysed (AR01 to AR05).

In the case of the first sample, the best estimation of the thermal diffusivity is obtained for the measurement point AR01, corresponding to the centre of the sample surface. For other measurement points, some deviations are observed; they are probably due to edge effects.

The identified value of the thermal conductivity is higher than the one reported in table 1; however, as we said before, diverse values of plaster thermal conductivity can be found in the literature, and this value is not abnormal for this kind of material [3].

We have reported in the right column of the table, an estimation of the thermal resistance of the first layer. This value was computed using the estimated value of the amplitude  $C$  and knowing the value of the absorbed density power  $P$ . This value of  $P$  was previously estimated by performing a comparison of the measured temperature profiles on the sample surface to computed temperature profiles obtained from numerical simulations (using FLUENT™). These simulations are not presented in this paper. This last procedure was also applied to the analysis of data obtained for the second sample.

**Table 2.** Identification results obtained for the first sample

Meas. point	$L$ mm	$Fo_e$	$C$ K	$NB$	$a$ $\times 10^{-7} \text{ m}^2/\text{s}$	$k$ $\text{W}\cdot\text{m}^{-1}\cdot\text{K}^{-1}$	$R$ for $P = 1303\text{W}/\text{m}^2$
AR01	10	0.23	51	0.73	4.31	0.51	1.96
AR02	10	0.31	45	0.72	5.65	0.58	1.73
AR03	10	0.34	41	0.60	6.33	0.64	1.57
AR04	10	0.28	45	0.76	5.12	0.57	1.75
AR05	10	0.33	44	0.66	6.11	0.59	1.68

Concerning the second sample, we observe a strong dispersion of the values of the thermal diffusivity. Estimated values of  $a$  are increasing as the plaster layer thickness increases. On the contrary, the estimated values of the thermal conductivity are less dispersed than the ones of the thermal diffusivity. Besides, we observe a continuous increase of the identified value of the thermal resistance of the

plaster layer between AR01 and AR05 point. This result was expected as the plaster layer thickness increases between these points.

**Table 3.** Identification results obtained for the second sample

Meas. point	$L$ mm	$Fo_e$	$C$ K	$NB$	$a$ $\times 10^{-7}$ m <sup>2</sup> /s	$k$ W.m <sup>-1</sup> .K <sup>-1</sup>	$R$ for $P = 975$ W/m <sup>2</sup>
AR01	6	23.9	21	0.15	4.78	0.55	1.08
AR02	10	9.2	36	0.23	5.1	0.56	1.85
AR03	14	4.9	54	0.34	5.35	0.5	2.77
AR04	18	3.2	74	0.49	5.71	0.47	3.79
AR05	22	2.5	91	0.63	6.84	0.47	4.67

#### 4.2 Semi-infinite body model

As described above, the objective is to determine a characteristic time, correlated to the presence of the interface between the plaster layer and the polystyrene layer. In figure 5, we present the evolution of identification residual norm as a function of the measurement time, for the five measurement points. We observe that for short times, the residual norm value is low. This values starts to increase dramatically after a given time  $t_c$ . We can also notice that this characteristic time is dependent on the measurement point, *i.e.* on the plaster layer thickness.

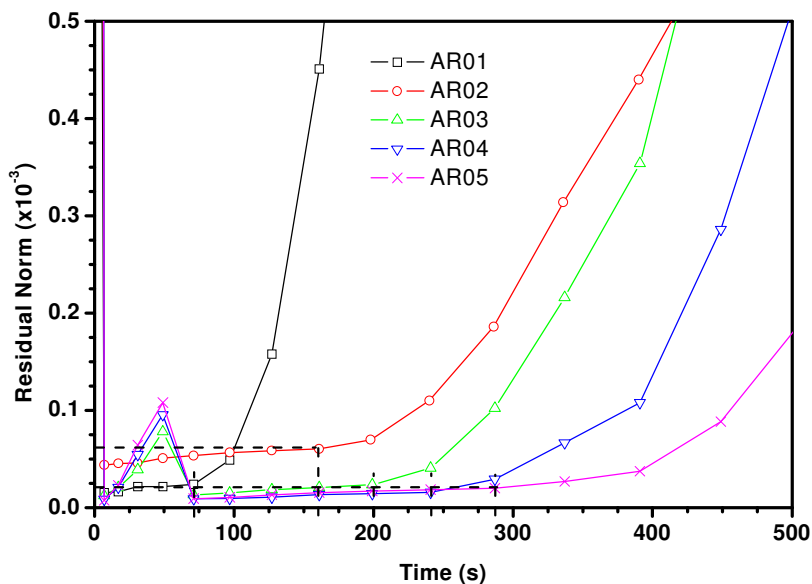


**Fig. 5.** Evolution of the identification residual norm upon time

A similar result is obtained if we follow the evolution of the product of the two estimated parameter ( $\alpha.\beta$ ). Using equation 10, we can deduce that this product is equal to  $P/e$ . So, we could expect this parameter to be constant and independent on the measurement time. The corresponding results are presented on figure 6. For very short measurement times, we obtain dispersed values of  $\alpha.\beta$ . This is probably due to the small number of experimental data. For longer times, we observe that this parameter remains quite constant. Finally, for times longer than  $t_c$ , we notice a strong variation of this parameter.

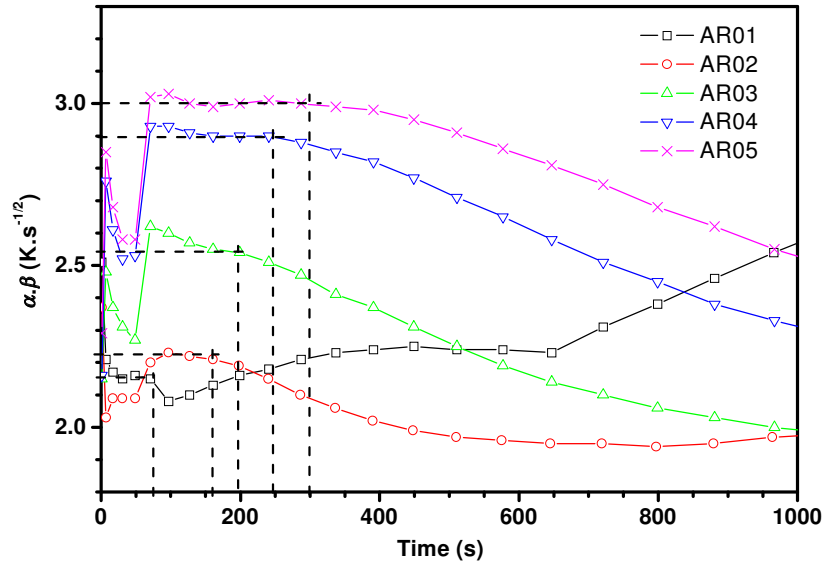


Fig. 6. Evolution of the product of estimated parameters  $\alpha.\beta$  upon time.

### 4.3 Estimation of the first layer thickness

The values of characteristic time  $t_c$  are plotted on figure 7 as a function of the theoretical thickness of the first layer. We can notice a linear dependence of this characteristic time upon layer thickness. On the basis of these results, we can try to obtain an estimation of the first layer thickness. This was performed as follows. A temperature profile along the position in the first layer thickness was done using equation 9 and the estimated values of  $\alpha$  and  $\beta$ . Then, the position of the interface was estimated using an arbitrary criterion, based on the value of the temperature gradient along the direction  $x$ :

$$\frac{\partial\theta(x,t)}{\partial x} \leq \eta \tag{12}$$

The values of the first layer thickness estimated using a value of  $\eta = 0.01$  are also plotted on figure 7 versus the theoretical thickness. We also observe here a linear relationship between the estimated and the theoretical thicknesses.

Nevertheless, we observe some discrepancies between the estimated and the theoretical values, especially for the smallest thicknesses.

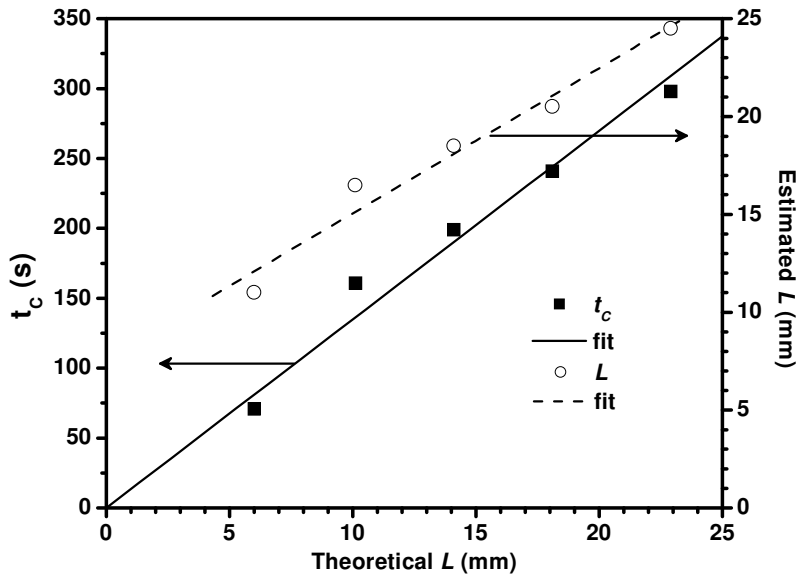


Fig. 7. Estimated values of the characteristic time  $t_c$  and of the first layer thickness  $L$ .

## 5 Conclusion

In this work, an experimental protocol was defined to determine the thermal resistance of the first layer of a multi-layered wall. The use of a heat transfer model considering an adiabatic interface allowed us obtaining an estimation of the thermophysical properties of the first layer. Besides, an estimation of the first layer thickness might be obtained using of a semi-infinite body model. Nevertheless, some discrepancies were observed between theoretical and estimated values. Future works should be focussed on the improvement of the estimation of these parameters in order to provide an accurate estimation of the thermal resistance.

## REFERENCES

- [1] D. MANUEL, S. OBLIN and P. RICHARD. Thermographie infrarouge appliquée à la détection de défaut d'isolation, Rapport final CSTB, ENEA/SES 98.128R, Paris, France, (2003).
- [2] M. LARBI YOUSSEF, S. DATCU, L. IBOS and Y. CANDAU. Analyse de l'état de l'art sur la mesure de la résistance thermique d'une paroi isolante en régime non permanent, Rapport d'étude CERTES/EDF, Paris, France, (2004).
- [3] RT 2000, Règles Th-U, Fascicule 2/5, CSTB, Paris, France, (2001).
- [4] S. DATCU, L. IBOS and Y. CANDAU. Square pulsed thermography applied to thermal default characterization, QIRT, Rhodes-St-Genève, Belgique (2004).
- [5] V. VAVILOV. Transient NDT : conception in formulae, QIRT, Paris, France, (1992).